Available online at www.sciencedirect.com
SCIENCE DIRECT®
ELSEVIER
Nuclear Instruments and Methods in Physics Research A 553 (2005) 114–119
NUCLEAR INSTRUMENTS & METHODS IN PHYSICS RESEARCH Section A
www.elsevier.com/locate/nima

Magnetic shielding studies of the LHCb rich photon detectors

M. Patel*, M. Losasso, T. Gys

CERN, Geneva, Switzerland

Available online 29 August 2005

Abstract

The LHCb experiment will use two RICH detectors to provide particle identification. The Hybrid Photon Detectors (HPDs) adopted for these detectors are required to operate in the fringe field of the 4 Tm LHCb dipole magnet. In fields in excess of 15 G, photoelectrons are lost from the active area of an HPD. Shielding the HPDs from the fringe field is therefore essential for the efficient operation of the RICH detectors. This paper describes the technique used to calculate the residual field inside the relevant magnetic shields. The size of the problem, together with the disparity in the geometric scales involved, makes the calculations intractable using a finite element model of the entire magnetic environment. As a result, a sub-modelling method has been used. The model indicates that the photon detectors will operate efficiently.

PACS: 25.6; 34.8a

Keywords: Magnetic shielding; Hybrid photon detectors

1. Introduction

The LHCb experiment [1] will make high precision studies of CP violation and other rare phenomena in B meson decays. Particle identification in the momentum range from a few to $\sim$100 GeV/c is essential for this physics programme. In order to provide this capability, two Ring Imaging CHerenkov (RICH) detectors will be employed [2].

The photon detector adopted for LHCb is the custom-made Pixel Hybrid Photon Detector (HPD). Details of the HPD construction can be found elsewhere [3]. The HPD characteristic relevant here is the sensitivity to magnetic fields: the two RICH detectors in the LHCb experiment are located either side of a 4 Tm dipole magnet (Fig. 1). The HPDs in the RICH detectors therefore experience a stray magnetic field and shielding is required to reduce the resulting magnetic distortions. The stray field is largest in the upstream detector (RICH1) which is closer to the magnet. The present paper therefore focuses on this detector.

*Corresponding author.
E-mail address: mitesh.patel@cern.ch (M. Patel).

0168-9002/$ - see front matter © 2005 Elsevier B.V. All rights reserved.
doi:10.1016/j.nima.2005.08.043

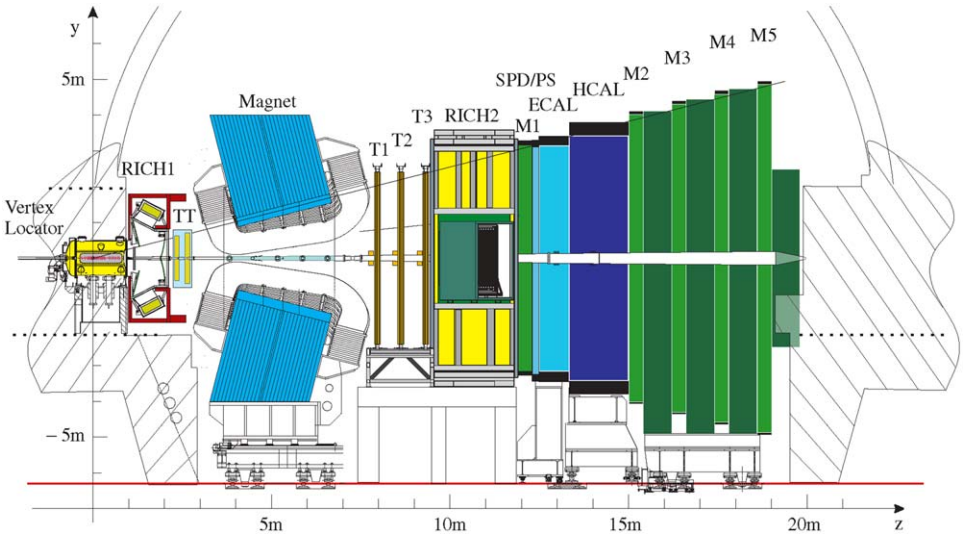

Fig. 1. Schematic of the LHCb detector.

In addition to shielding the HPDs, the magnetic shield around RICH1 must also deliver flux into the region between two tracking stations, the 'Vertex Locator' and the 'Trigger Tracker', which are located either side of it. This allows an estimate of the momentum of charged tracks to be made which is essential for the LHCb trigger. A primary iron magnetic shield that, as far as possible, satisfies the conflicting shielding and flux delivery constraints has been developed (Fig. 2) [4].

Photoelectrons are lost from the active region of an HPD in magnetic fields in excess of 15 G. Finite element (FE) calculations, made using the OPERA-3d software [5], indicate that the residual field inside the primary RICH1 magnetic shield is ~20 G [6]. In order to reduce this to a level where no photoelectrons are lost, individual secondary shields will enclose each HPD. In each half of the RICH1 detector, an array of 14×7 cylindrical secondary shields, each ~80 mm in diameter, 140 mm long and nominally 0.9 mm thick, will therefore be enclosed within the primary magnetic shield (Fig. 3).

The primary shield has dimensions ~(2 m × 1 m × 1 m) and is adjacent to the large (11 m × 4 m × 2.5 m) dipole magnet (Fig. 4). The shapes and the differing geometric scales result in a large number of elements being required to construct an FE model of this environment. The elements must also extend into a volume that encompasses not just the detector, but also the majority of the field.

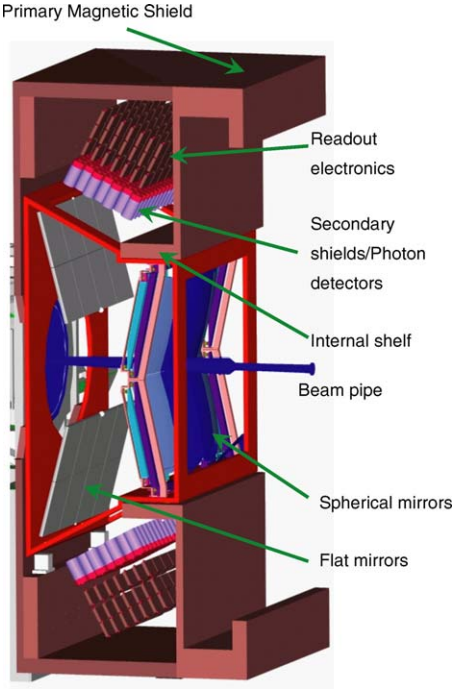

Fig. 2. The RICH1 detector.

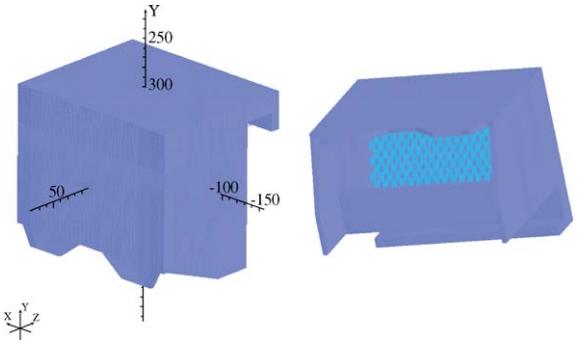

Fig. 3. The RICH1 magnetic shield. The tilted view (right) shows the 14×7 array of secondary magnetic shields.

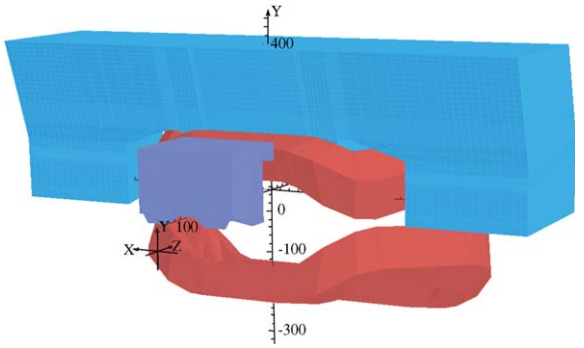

Fig. 4. Half-symmetry OPERA-3d model of the RICH1 primary magnetic shield and the magnet.

Consequently, FE models of the primary shield and the magnet, without the secondary shield array, already use the total number of available elements. Extension of the existing FE models to include the secondary shields is technically unfeasible without sub-modelling.

A calculation including the secondary shield array is highly desirable for the following reasons: to ensure that the introduction of high permeability secondary magnetic shields does not result in the magnetic flux 'short circuiting' through the detector array; to ensure that the residual field inside each HPD shield is $<15\,\mathrm{G}$; and that the secondary shield material is far enough from saturation such that any additional flux, not predicted in the simulation, does not result in field leaking into the active HPD volume.

2. Sub-modelling

In order to calculate the field inside the primary shield, a 'complete model', containing the elements required to form both the magnet and the primary shield, was first solved using an OPERA-3d FE model.

The magnetic potential was extracted from this solved complete model in a region around the primary shield but excluding the magnet. The boundary of this part of the complete model was chosen such that the potential at its surface boundaries was not expected to change when the secondary shields were introduced. The potential was then applied to a new, part model, with the same boundary, containing the primary magnetic shield and the secondary shield array, but not the magnet. The much smaller volume of this model allowed many more elements to be used to form the secondary shields.

After the application of the boundary potential from the complete model, the part model was then solved again with the potential fixed at the boundaries but allowed to evolve elsewhere. Solutions were obtained first with the secondary shield array made of air, in order to understand the effect of the choice of element size and the error introduced by the use of the sub-modelling process (found to be $<1\%$); and then with the secondary shield array made of a high permeability material. In the latter case two candidate materials were simulated: 'MuMetal' and 'Supranhyster-36'.[1] Both materials are nickel–iron-based alloys with maximum relative permeabilities of 4×10^5 and 1×10^5 and saturation values of 7 and 11 kG, respectively.

Despite using the sub-modelling approach, the limited number of elements available resulted in the secondary shield array being approximated by square rather than circular shaped shields. Maintaining the same inter-shield pitch, this resulted in a model with $\sim$10% more shield material in the simulation than will be in the real shield array. However, the model predicts shield material sufficiently far from saturation such that this

[1] MuMetal is a trademark of Telcon, Supranhyster-36 a trademark of Imphy Alloys.

additional material does not affect the results presented here.

The potential from the solved part model was compared to that from the complete model. The perturbation caused by the introduction of the secondary shields was found to be small and confined well within the model, away from the boundaries where the method fixes the potential.

3. Results

3.1. The field at the detector plane

MuMetal shields of thickness 0.9 mm were modelled and result in the maximum field inside the HPD volume falling from ~20 to 8 G.

The modulus of the field at the HPD plane is shown with and without the MuMetal in Fig. 5. The field along several lines, parallel to the HPD plane, is shown in Fig. 6. The lowest fields in the active volume of an HPD are observed at the edge of the shield array; the largest fields are observed at the centre of the array.

The field predicted across the central region of the HPD plane is shown in Fig. 7. With shields made of MuMetal, flux is channelled through the shield material, leaving regions of low field where the HPDs will be situated. In contrast, in the absence of the shields (shield material air) the open geometry results in the flux from the magnet flaring into the open edge of the primary shield, exactly at the position of the HPD array (Fig. 8).

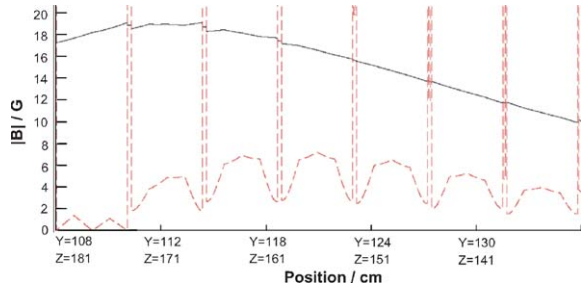

Fig. 5. Modulus of the field along a line through the central seven shields for shields composed of air (solid line) and MuMetal (dashed line).

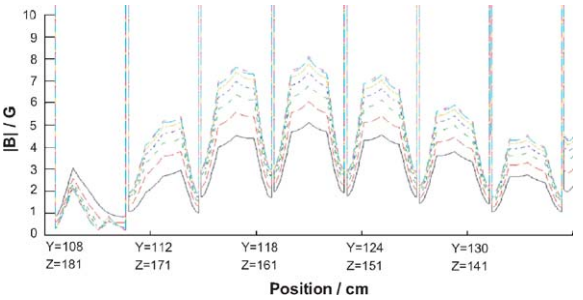

Fig. 6. Modulus of the field along lines through each set of shields from the edge of shield array (lowest fields) to the centre of the array (highest fields).

The much smaller field seen in the lowest shields in the array owes to the proximity of these shields to the internal shelf of the primary iron shield (see Fig. 2). The field in this region has the most significant component transverse to the axis of the HPDs and is therefore better shielded. In the other shields the field is mostly longitudinal.

3.2. Field inside the shield material

Using 0.9 mm-thick shields, the internal fields observed in the MuMetal are typically ~2 kG. A peak field of 3.9 kG is observed at the lower edges of the array, where the shields are closest to the side walls and internal shelf. MuMetal saturates at fields of 7 kG and the array is therefore significantly away from saturation.

3.3. Supranhyster-36 shield array

The part model was also solved using the permeability curve of the material Supranhyster-36 rather than that of MuMetal. Although this is a lower magnetic permeability material, the permeability is so much higher than that of air that identical shielding performance is obtained. Supranhyster-36 saturates at 11 kG. Since the peak fields observed are similar to those for MuMetal, the shields are therefore even further away from saturation.

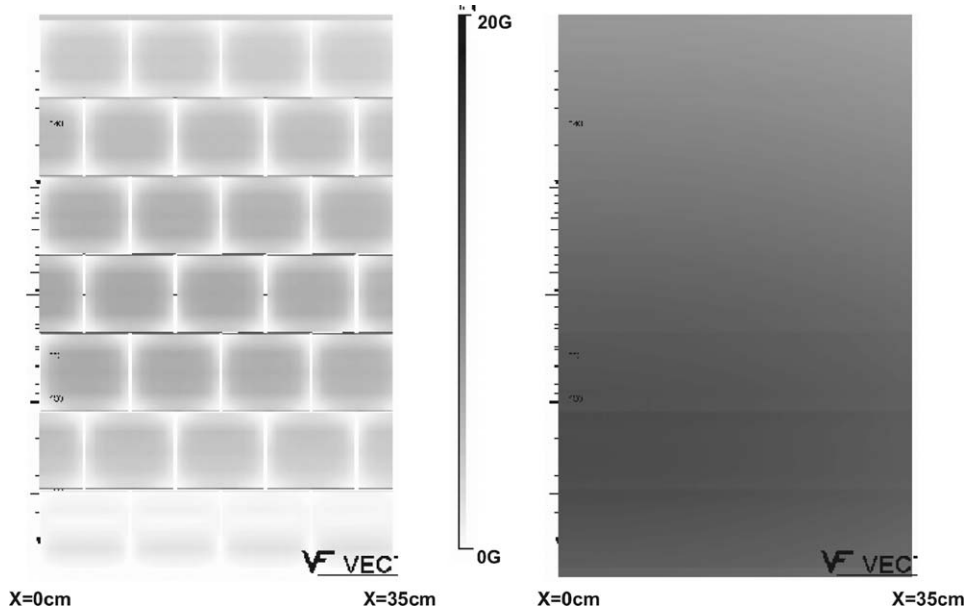

Fig. 7. Field distribution across the central region of the HPD plane for a model with MuMetal secondary shields (left) and with air secondary shields (right). The full 7 rows of shields are shown but only 4 of the 14 HPDs.

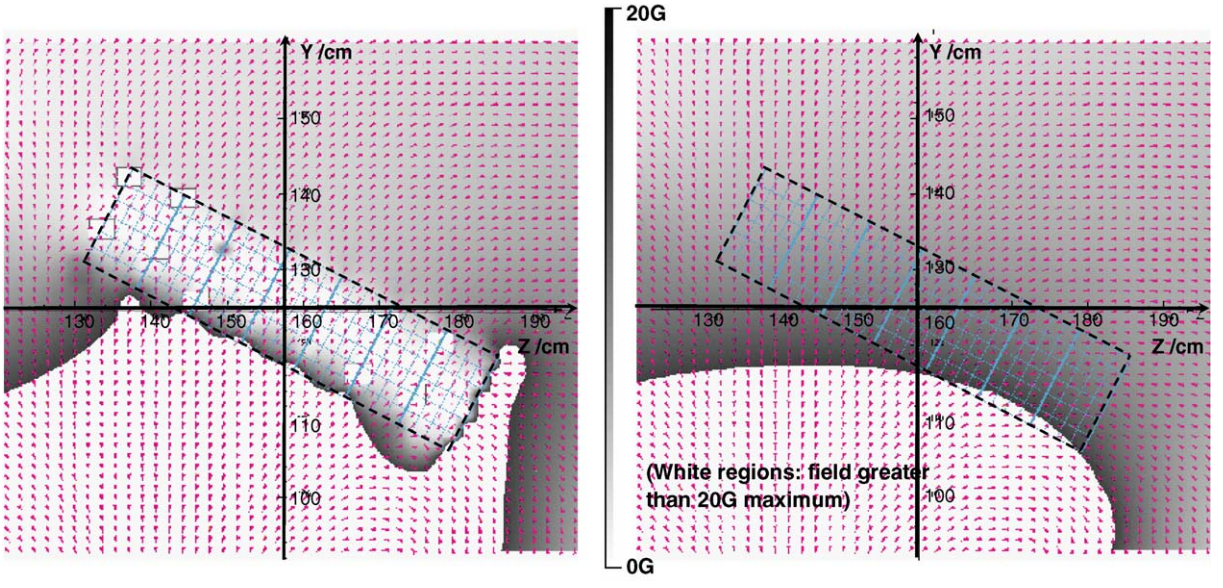

Fig. 8. Field lines inside the primary magnetic shield (y–z plane at $x = 0$) for a model with MuMetal secondary shields (left) and with air secondary shields (right).

4. Conclusions

An FE calculation of the magnetic field in the region of the photon detectors in the upstream LHCb RICH detector has been made. The complicated geometry and the various scales involved required the use of a magnetic sub-modelling technique to simulate the magnetic

environment. The individual secondary shields around each of the photon detectors result in fields in the active region of the HPDs being reduced from ~20 to <8 G. The field is mostly longitudinal to the HPD axes, apart from the set of HPDs closest to the internal shelf of the primary iron magnetic shield. In these latter shields, the field is transverse to the HPD axes and is therefore attenuated much more than in the longitudinal case. The peak field observed in the shield material is approximately half way from the saturation value of the candidate shield material MuMetal (7 kG); and even further from saturation in the material Supranhyster-36 (11 kG). The latter gives similar shielding performance, despite its lower magnetic permeability.

The magnetic environment in the upstream RICH detector is therefore such that the photon detectors will operate without the loss of photoelectrons from their active area. A method of mapping the residual field in situ and compensating for the magnetic distortions is reported elsewhere in these proceedings [7].

References

[1] The LHCb Collaboration, LHCb Technical Proposal, CERN-LHCC-98-4, CERN, 1998.
[2] The LHCb Collaboration, LHCb RICH Technical Design Report, CERN-LHCC-2000-037, 2000.
[3] M. Moritz, et al., IEEE Trans. Nucl. Sci. NS-51 (3) (2004) 1060.
[4] The LHCb Collaboration, LHCb Reoptimized Detector Design, CERN-LHCC-2003-030, 2003.
[5] Vector fields ⟨http://www.vectorfields.com⟩.
[6] R. Plackett, et al., Private communication, 2004.
[7] G. Aglieri Rinella, et al., these proceedings.